Switchable metal-insulator phase transition metamaterials

*Ghazal Hajisalem, Mohammadreza S. Nezami, Reuven Gordon**

Department of Electrical and Computer Engineering, University of Victoria, Victoria, BC, Canada, V8P 5C2

KEYWORDS: Phase transition materials, metamaterials, second and third harmonic generation, quantum tunneling, plasmonics, self-assembly.

ABSTRACT: We investigate the switching of a gap plasmon tunnel junction between conducting and insulating states. Hysteresis is observed in the second and the third harmonic generation power-dependence, which arises by thermally induced disorder ("melting") of a 2-carbon self-assembled monolayer between an ultra-flat gold surface and metal nanoparticles. The hysteresis is observed for a variety of nanoparticle sizes, but not for larger tunnel junctions where there is no appreciable tunneling. By combining quantum corrected finite-difference time-domain simulations with nonlinear scattering theory, we calculate the changes in the harmonic generation between the tunneling and insulating states, and good agreement is found with the experiments. This paves the way to a new class of metal-insulator phase transition switchable metamaterials, which may provide next generation information processing technologies.

At the end of Moore's law, many are looking to photonic technologies to replace electronics [1], yet the challenge has been finding functional materials with an energy-efficient and large change in their optical response. The metal-insulator transition provides an extremely strong change in optical properties and therefore it is highly sought after for future photonic information processing technologies [2]. Unfortunately, only limited materials are available that can be used for such applications. Here we present an artificial metamaterial that is designed to undergo a metal-insulator transition and gives ~60% change in the third harmonic generation. This demonstration provides a platform for future generation highly-efficient optical information processing technologies.

Phase transition materials have the interesting property of allowing for large changes in the optical response, which is potentially useful for optical switching applications [1,3]. The large switching comes as a result of the difference between the conducting state (that screens out the electric field) and the insulating state (that lets an electromagnetic wave propagate). Vanadium dioxide is probably the most promising conventional example of this transition with strong optical response near room temperature and there have been many demonstrations of using this in switching applications [4,5]. Recently, grating structures have been introduced using defect engineering in vanadium dioxide [6]. Also, vanadium dioxide has been combined with plasmonics to obtain a greater switching response [7,8]. Greater functionality has also been achieved in other phase change material based metasurfaces [9]. Among conventional materials, however, there are limited examples that can be effectively used in optical switching applications.

Here we consider a designer approach to phase transition based switching. We borrow from the technology of metamaterials, where a material is artificially constructed to have desired

optical characteristics not found in conventional materials. In particular, we make use of the plasmonic nanosphere over metal film structures, where a self-assembled monolayer (SAM) of amine-terminated alkanethiols provides a controlled spacer layer [10]. (SAMs are not the only way to achieve tunable gap length; for example, electrical tuning of an oxide layer has been demonstrated in a similar geometry as shown here [11]). The optical response is largely governed by the gap-size of the spacer layer, and there is an abrupt change when reducing the SAM from the tunneling to insulating regimes [12]. This sudden change in the optical properties is not unique to SAM systems [13,14].

In the past, we have explored the tunneling and insulating regimes by varying the length of the molecules in the SAM [12]; however, here we explore the ability to change the length of a SAM by a phase transition to the disordered state for a single sample. In this way, we demonstrate that it is possible to transition between the tunneling state (metal) to the insulator state, which has a great impact on the optical response by modulating the gap plasmon of the metal-insulator-metal junction. This work follows recent interest in switchable metamaterials [15,16]; however, we believe that this is the first demonstration of metal-insulator switching allowed by such a platform for next generation information processing technologies such as optical buffers and memory, optical logic (although presently slow), and switching [1,16].

Figure 1 shows the third harmonic response of the metal nanoparticles over an ultra-flat gold film for 2 carbon (C2) and 3 carbon (C3) SAMs. A variety of particle sizes were investigated, yet they all showed similar trends, indicating that the differences in behavior are the result of modulation to the SAM. The C3 shows saturation in the nonlinear response at higher powers, which is common for nonlinear materials. The C2 sample, however, shows a jump when increasing the power, and does not follow the same dependence when reducing the power. This

was early data where we first discovered hysteresis for all particle sizes of C2 – we then went back and did thorough characterization for a single size to better understand the effect.

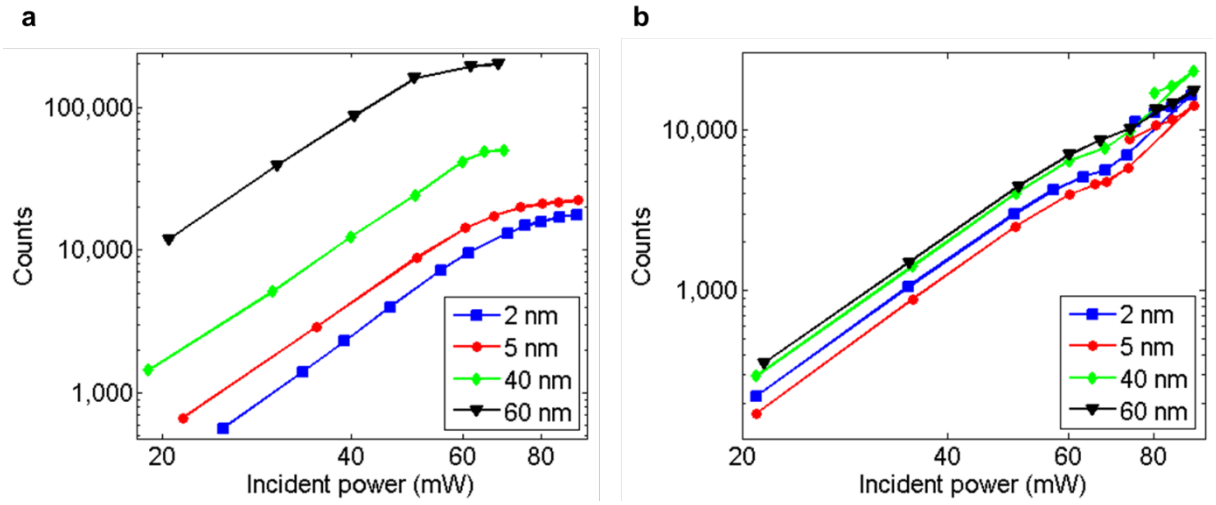

Figure 1. THG response as a function of incident power for varying diameter gold nanoparticles on top of a gold film. (a) THG responses of samples with three carbons SAM, the power-law dependence of THG signals gives slope of ~3 ± 0.2 on a log-log plot when incident power varies between 19 mW and ~60 mW, further increase of the incident power results in saturation of the THG signal for all samples. (b) THG responses of samples with two carbons SAM shows a jump when increasing the power and does not follow the same dependence when reducing the power.

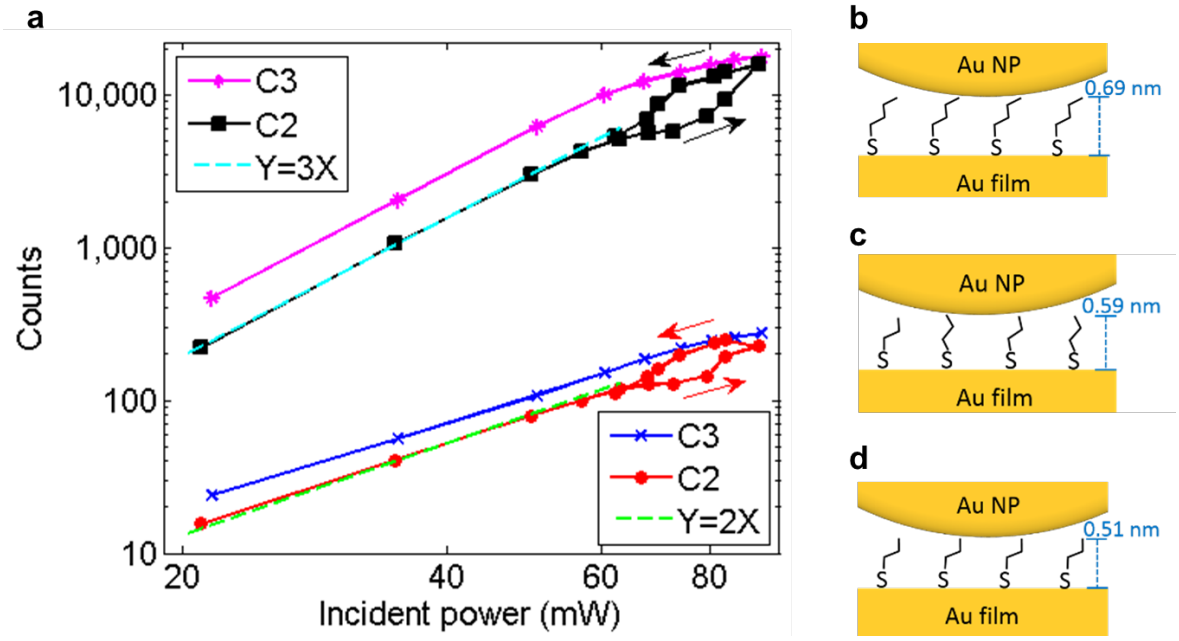

Figure 2. Second and third harmonic responses as a function of the incident power. (a) By increasing the incident power above ~60 mW, nonlinear responses of a C3 sample saturates, whereas nonlinear responses of a C2 samples show a sudden jump up and hysteresis loop. Schematics (b-d) show estimate length of SAMs for a sample of gold nanoparticles-over-gold film separated by (b) a SAM of C3, (c) a disordered SAM of C2, and (d) an ordered SAM of C2. Y = 2X and Y = 3X are fitted lines to the log-log plots of THG and SHG with slope of ~3.0 ± 0.1 and SHG is ~1.9 ± 0.1, respectively.

For large gold nanoparticles, applying incident powers higher than ~60 mW can result in sample damage for C3 [12]. In this case, as we have previously reported with a video in the Supporting Information of Ref. 12, sudden "explosions" in the intensity of the light emitted from the region of the nanoparticles when translating over the sample and a significant drop of the THG signal, around 90%, was observed. Therefore, here we compare for 2 nm particles the C2 and C3 sample nonlinear optical response. Figure 2 shows the second harmonic and third harmonic power-dependence response of the C2 with a clear hysteresis seen for both curves. The

hysteresis has been reproduced extensively on different samples and in different locations of the same sample (see Supporting Information).

We propose a mechanism for this switchable response: at higher incident intensities, the SAM layer undergoes a thermally induced phase transition to a disordered state. This disordered state increases the size of the SAM [17] and thereby switches the material from a tunneling gap (conductor) to an insulating gap. The insulating gap allows for greater field in the gap and thereby a greater nonlinear response. The different gap sizes for the C3, C2 (disordered) and C2 (ordered) are shown in Figures 2b-d. Here we used theoretical heights [10] of SAMs where the ordered C2 and C3 SAMs are 30^{o} tilted relative to the normal of the surface and the disordered C2 has 0^{o} tilt angle [17].

Other works have noted that SAMs undergo a disordering phase change ("melting") at relatively low temperatures (around 330 K to 390 K) [17,18]. This is comparable to the phase transition temperature in VO_2 samples [6,19]. To explore further the phase transition dynamics, we increased the laser power (up to 91 mW) and then promptly reduced it to 70 mW, a power within the hysteresis loop. We then observed a slow decline in nonlinear response to the lower branch of the hysteresis loop, consistent with "freezing" back into the ordered SAM state. In Figure 3a the time interval for changing power was 30 seconds between each measurement. Figure 3b shows the decay observed in the third and second harmonic response, with a time constant of the order of 10-15 minutes, which is an appropriate order of magnitude for such "freezing". This has been repeated on different samples (see Supporting Information). From Figures 3b and 1Sb, we estimate that the SAMs recovery time is between 10 and 15 minutes. However, we did not see the transition from ordered to disordered state on the timescale of our measurement (~10 s); therefore, it is expected that melting is a faster process than ordering. Also,

the peak in the Figure 3b at around 9 minute is due to experimental error. We repeated this measurement several times and did not see the peak in other instances, for example, see the Supporting Information.

We estimate the temperature increase under 80 mW irradiation using the approach of Ref. 20. The temperature increase of a laser-irradiated film over a substrate is calculated by numerical integration of Equation A12 in that reference. Using the parameters of 100 nm for the gold film thickness, 3 microns for the laser spot size, 314 W/(mK) for the gold thermal conductivity, 0.17 W/(mK) for the substrate thermal conductivity (obtained from Norland for NOA61) and 3% for the absorption coefficient (slightly higher than regular gold due to the nanoparticles), we find a temperature increase of 47 K. Considering room temperature of 293 K, this gives a local temperature of 340 K, which is just above the SAM melting temperature of 330 K reported in the literature [17] but well below the thermal damage threshold [21].

To explore quantitatively the switchable nonlinear response further, we employed a quantum corrected model (QCM) in finite-difference time-domain (FDTD) with varying gap width [12,22]. The gap was modeled using a Drude material with transport properties extracted from the DC tunneling rate [23]. We used a nonlinear scattering theory to obtain the nonlinear response [24]. Figure 4 shows the response for gaps of 0.51 nm, 0.59 nm, and 0.69 nm, where total electric field intensity profiles at 1570 nm are calculated in the metal film just below the nanoparticle. It is clear from this figure that for the shortest gap, the ordered C2, a hole emerges in the center of the gap due to tunneling beginning to short out the junction. Whereas disordered state increases the gap size and thereby switches the tunneling to insulating regimes.

Table 1 summarizes the quantitative findings of the QCM model in comparison to the experiments, with reasonable agreement (especially considering that no *a posteriori* fitting was performed).

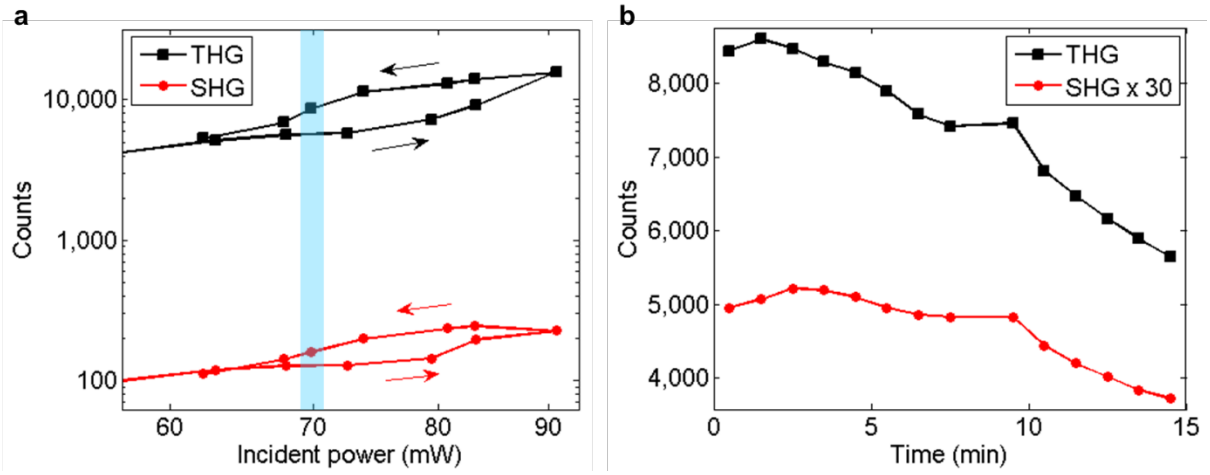

Figure 3. SHG and THG responses as a function of incident power and time. (a) THG and SHG responses of the sample with two carbons SAM shows sudden jump and hysteresis loop. We attribute the sudden jumps to an induced disorder of C2 SAM layer due to applying high incident power. (b) Shows the time evolution of the nonlinear response of C2 sample at 70 mW incident power.

This switchable nonlinear response is interesting for optical switching applications. In particular, a control pulse can be used to modify the phase of a signal pulse and switch its direction, which is the common optical switching configuration [25]. Typically, the Kerr response is used to obtain the switching. Here, we do not attempt the Kerr switching measurement, however, the third order susceptibility that governs the Kerr response also gives rise to the third harmonic generation observed in our measurements [26,27]. It is interesting to note that third harmonic is switched by up to 60% (at incident power ~73 mW). Of course, in our present geometry, the nonlinear response is coming only from a sparse distribution of

nanoparticle gaps (areal coverage of 0.19 ± 0.02 %) – it is reasonable to anticipate that increasing the density and optimizing the design will result in even larger responses being recorded. It is possible that different materials could result in a larger change in the gap size, thereby increasing the switching ratio – for example, perhaps with photoisomerization this could be achieved [28,29]. This is also promising for faster speeds. Of course, the present phase transition has a slow thermal time-constant and therefore would be too slow for ultra-fast switching applications. Although this is slow, it can be used for reconfiguring optical networks where MEMS are used now [1,9,16]. Another possible application is as an optically addressable buffer. Ideally, future work would investigate faster switching mechanisms. Nevertheless, the present demonstration shows the concept of phase transition metamaterials, and even if faster transitions are not found, may still be of interest to slower memory and routing applications.

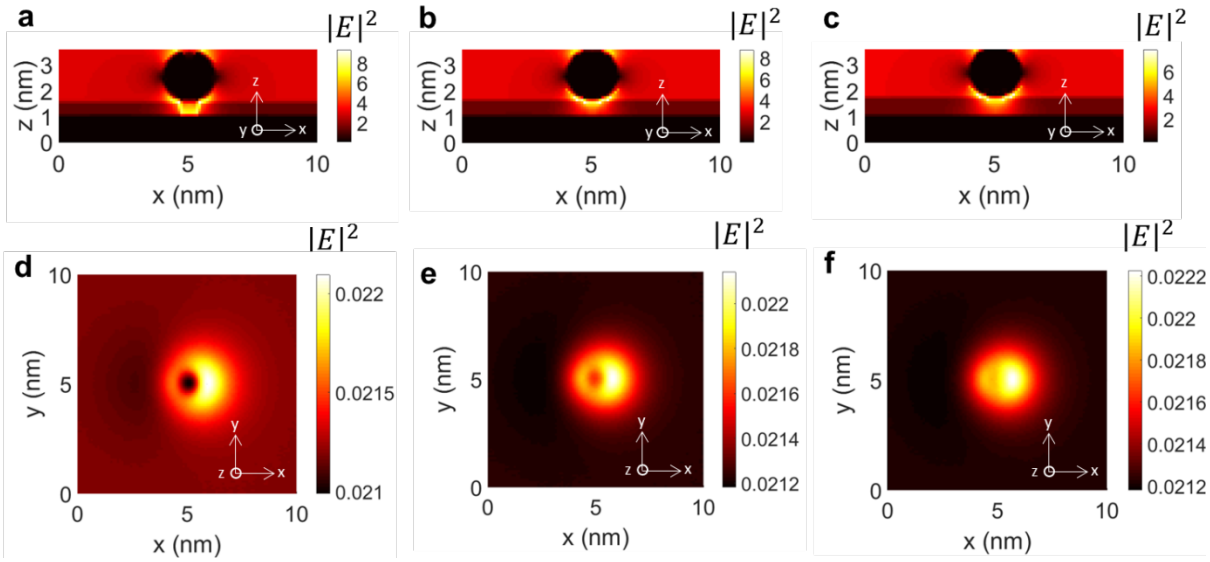

Figure 4. Total electric field intensity profiles in the metal film just below the nanoparticle plane for different spacer thicknesses at wavelength 1570 nm, calculated by QCM. (a) Cross section and (d) spatial profiles for ordered C2 SAM layer with 0.51 nm thickness. (b) Cross section and

(e) spatial profiles for disordered C2 SAM layer with 0.59 nm thickness. (c) Cross section and (f) spatial profiles for ordered C3 SAM layer with 0.69 nm thickness.

Table 1. The QCM model in comparison to the experiments. [a]The plasma frequency inside the gap.

spacer type	ω_g (rad/sec)[a]	normalized SHG		normalized THG	
		simulation	experiment	simulation	experiment
C2	2.4×10^{15} [b]	0.79	0.78	0.65	0.56
C2 disordered	1.75×10^{15} [c]	0.9	0.99	0.81	0.88
C3	1.1777×10^{15} [b]	1	1	1	1

[b]Calculated by us in Ref. 12. [c]Calculated by using the method from Ref. 12 and Ref. 22.

In summary, we have presented an artificial metamaterial that undergoes a metal-insulator phase transition and therefore shows an extremely large modulation in the optical response. We anticipate that improved optical design will result in higher performance from SAM-based metamaterials, or others that can produce modulation in a plasmonic tunneling gap. Because tunneling is exponentially sensitive to gap distance, we believe that this is a promising route to energy efficient optical materials for future generation photonic information processing.

Methods. *Sample preparation:* We used samples of gold nanoparticles on top of ultra-flat gold film with SAM spacer layers, prepared with the same method as our previous work12. Ultra-flat gold films were fabricated by evaporating 30 nm of gold onto silicon wafers at a rate of 1 Å/s and temperature of 200 ˚C. Promptly, the gold slides were coated with a thin layer of optical epoxy (Norland Optical Adhesive 61) followed by a clean glass slide. The epoxy was cured by UV light for 5 min. The gold film was "stripped" from the silicon wafer, revealing the ultra-flat

surface of gold film. To fabricate SAMs of C2 and C3 on the fresh ultra-flat gold films, 2mM solutions of amine-terminated alkanethiols of cysteamine (30070, Sigma Aldrich) and 3-amino-1-propanethiol hydrochloride (739294, Sigma Aldrich) in ethanol were prepared, respectively. SAMs were formed by immersing the ultra-flat substrate into the alkanethiol solution for 18 h, followed by sonication for 2 min and rinsing with ethanol for 15 seconds. The process of sonication and rinsing was repeated four times. Finally, the substrate was dried using nitrogen gas. Samples with 2 nm, 5 nm, 40 nm, and 60 nm nanospheres (BBI) on top of the SAMs were fabricated by incubating 500 µl of the colloidal stocks for 30 min followed by rinsing with deionized water (USF Elga, Maxima, model Scientific MK3, 18.2 MΩ-cm) for 15 seconds and drying with a stream of nitrogen gas.

THG/SHG measurement: The nonlinear optical properties of samples were studied by using the same method as our previous work [12] with a 100 fs 1570 nm fiber laser module (Mercury 1550-100-MOD, PolarOnyx), 38 MHz pulse repetition rate. A longpass filter was used to remove weak second harmonic and third harmonic signals generated prior to the sample. Also, S-polarization of the source was minimized by passing the beam through a half wave plate and a linear polarizer. The source power was adjusted between 19 mW and 91 mW by using a continuously variable neutral density filter (Thorlabs) and measured before focusing onto the sample. The source beam was aligned off-center of the 50× microscope objective (0.85 NA, Melles Griot), focusing onto the sample. The reflected source beam was filtered using a shortpass filter, and the scattered beam was directed into a spectrometer (QE65000, Ocean Optics) for second harmonic and third harmonic measurements.

QCM simulation details: To mimic the quantum electron tunneling in the gap region of the nanosphere-assembled thin film, we used QCM similar to our past work [12]. Standard transmission coefficient was used for $E_f < V$:

$$T(d) = \left(\frac{1}{1 + \frac{1}{4} \frac{V^2 \sinh^2(\alpha \kappa d)}{\alpha E_f (V - E_f)}} \right) \quad (1)$$

$$V = E_f + \varphi_B \quad (2)$$

$$\kappa = \frac{\sqrt{2m\varphi_B}}{\hbar} \quad (3)$$

The plasma frequency inside the gap can be derived from [22]:

$$\omega_g(d) = \sqrt{T(d)}\omega_{pAu} \quad (4)$$

We set the scattering rate equal to that of gold $\gamma_g = 4 \times 10^{13}$ (red/sec) as a fixed value which is equal to the collision frequency of gold. Here φ_B is the barrier height, E_f is Fermi energy, α is the ideality factor that accounts for deviation from rectangular barrier shape, m is the electron mass, κ is the electron wave vector in the barrier, V is the barrier height plus the Fermi energy (i.e., the total energy) and $\hbar$ is the reduced Planck constant. The values:

$$\alpha = 0.65, V = E_{fAu} + \varphi_{B-SAM} = 5.53 \text{ eV} + 1.42 \text{ eV} = 6.95 \text{ eV} \quad (5)$$

The radius of QCM cylinder that we previously used for 60 nm nanoparticle was 1.5 nm. If the cross section area of the QCM cylinder scales down by a factor of R/R60, a QCM cylinder of 0.27 nm is suitable for a 2 nm particle.

We used Lumerical FDTD Solutions VER. 8.16.982. A total-field scattered-field (TFSF) source at an angle 50 degree illuminates the structure. A SAM layer with a refractive index of 1.5 was placed in the gap region between 2 nm gold nanosphere and a 30 nm gold film. A mesh override region was used over the x, y, and z span of the source. 0.1 nm mesh size was chosen for the simulation. Three QCM cylinders with the minimum radius of 0.3 nm was used to model

the electron tunneling in the gap region. We used perfectly matched layer (PML) boundary conditions in all directions. Three 3D field monitors collected electric field data at 1570 nm, 523 nm, and 785 nm. A 3D index monitor collected the data points of the refractive index of the structure at the fundamental wavelength. We used refractive index data to make overlay masks. These masks were used for discrimination of the metal region from the rest of the structure. The nonlinear scattering theory can be used to calculate SHG and THG. These nonlinear responses can be estimated by integrating the overlapping linear fundamental and harmonic fields over the metal region [30]:

$$\text{THG} \propto \int_{Au} \chi_{Au}^{(3)} \boldsymbol{E_{3\omega}}.\boldsymbol{E_{\omega}^{3}}\ dV \tag{6}$$

$$\text{SHG} \propto \int_{Au} \chi_{Au}^{(2)} \boldsymbol{E_{2\omega}}.\boldsymbol{E_{\omega}^{2}}\ dS \tag{7}$$

Where $\chi_{Au}^{(3)}$ the third order susceptibility of gold, $\chi_{Au}^{(2)}$ is the second order susceptibility of gold, $\boldsymbol{E_{3\omega}}$ is the linear third harmonic electric field vector, $\boldsymbol{E_{2\omega}}$ is the linear second harmonic electric field vector, and $\boldsymbol{E_{\omega}}$ is the linear fundamental electric field vector.

ASSOCIATED CONTENT

Supporting Information Available: Nonlinear optical responses of different samples, SEM image and linear optical measurements, and additional QCM simulation details. This material is available free of charge via the Internet at http://pubs.acs.org.

AUTHOR INFORMATION

Corresponding Author

*Email: rgordon@uvic.ca

Author Contributions

GH fabricated the samples, performed the experiments and analyzed the data. MSN performed the calculations. RG conceived of the project and assisted in data analysis.

Funding Sources

Funding is provided by the NSERC Discovery Grant program.

Notes

The authors declare no competing financial interest.

ACKNOWLEDGMENT

The authors acknowledge funding from the NSERC Discovery Grant program.

ABBREVIATIONS

SAM, self-assembled monolayer; C2, amine terminated alkanethiol of cysteamine; C3, amine terminated alkanethiol of 3-amino-1-propanethiol hydrochloride; SHG, second harmonic generation; THG, third harmonic generation; FDTD, finite-difference time-domain, QCM, quantum corrected model; TFSF, total-field scattered-field; PML, perfectly matched layer.

REFERENCES

(1) Zheludev, N. I.; Kivshar, Y. S. *Nat. Mater.* **2012,** 11, 917-924.

(2) Yang, Z.; Ko, C.; Ramanathan, S. *Annu. Rev. Mater. Res.* **2011,** 41, 337-367.

(3) Dionne, J. A.; Diest, K.; Sweatlock, L. A.; Atwater, H. A. *Nano Lett.* **2009,** 9, 897-902.

(4) Roach, W. R.; Balberg, I. *Solid State Commun.* **1971,** 9, 551-555.

(5) Joushaghani, A.; Jeong, J.; Paradis, S.; Alain, D.; Aitchison, J. S.; Poon, J. K. *Appl. Phys. Lett.* **2014,** 104, 221904.

(6) Rensberg, J.; Zhang, S.; Zhou, Y.; McLeod, A. S.; Schwarz, C.; Goldflam, M.; Liu, M.; Kerbusch, J.; Nawrodt, R.; Ramanathan, S; Basov, D.N.; Capasso, F.; Ronning, C.; Kate, M. A. *Nano Lett.* **2016,** 16, 1050-1055.

(7) Ferrara, D. W.; Nag, J.; MacQuarrie, E. R.; Kaye, A. B.; Haglund, Jr. R. F. *Nano Lett.* **2013,** 13, 4169-4175.

(8) Lei, D. Y.; Appavoo, K.; Ligmajer, F.; Sonnefraud, Y.; Haglund Jr, R. F.; Maier, S. A. *ACS Photonics* **2015,** 2, 1306-1313.

(9) Wang, Q.; Rogers, E. T. F.; Gholipour, B.; Wang, C. -M.; Yuan, G.; Teng, J.; Zheludev, N. I. *Nat. Photon.* **2016,** 10, 60-65.

(10) Hill, R. T.; Mock, J. J.; Hucknall, A.; Wolter, S. D.; Jokerst, N. M.; Smith, D. R.; Chilkoti, A. *ACS Nano* **2012,** 6, 9237-9246.

(11) Lumdee, C.; Toroghi, S.; Kik, P. G. *ACS Nano* **2012,** 6, 6301-6307.

(12) Hajisalem, G.; Nezami, M. S.; Gordon, R. *Nano Lett.* **2014,** 14, 6651-6654.

(13) Savage, K. J.; Hawkeye, M. M.; Esteban, R.; Borisov, A. G.; Aizpurua, J.; Baumberg, J. J. *Nature* **2012,** 491, 574-577.

(14) Scholl, J. A.; Garcia-Etxarri, A.; Aguirregabiria, G.; Esteban, R.; Narayan, T.C.; Koh, A.L.; Aizpurua, J.; Dionne, J. A. *ACS Nano* **2015,** 10, 1346-1354.

(15) Zhu, W. M.; Liu, A. Q.; Zhang, X. M.; Tsai, D. P.; Bourouina, T.; Teng, J. H.; Zhang, X. H.; Guo, H. C.; Tanoto, H.; Mei, T.; Lo, G.Q; Kwong, D. L. *Adv. Mater.* **2011,** 23, 1792-1796.

(16) Ou, J. Y.; Plum, E.; Jiang, L.; Zheludev, N. I. *Nano Lett.* **2011,** 11, 2142-2144.

(17) Ramin, L.; Jabbarzadeh, A. *Langmuir* **2011,** 27, 9748-9759.

(18) Schreiber, F.; Gerstenberg, M. C.; Dosch, H.; Scoles, G. *Langmuir* **2003,** 19, 10004-10006.

(19) Ladd, L. A.; Paul, W. *Solid State Commun.* **1969,** 7, 425-428.

(20) Burgener, M. L.; Reedy, R. E. *J. Appl. Phys.* **1982**, 53, 4357-4363.

(21) Stettner, J.; Winkler, A. *Langmuir* **2010**, 26, 9659-9665.

(22) Esteban, R.; Borisov, A. G.; Nordlander, P.; Aizpurua, J. *Nat. Commun.* **2012,** 3, 825.

(23) Wang, W.; Lee, T.; Reed, M. A. *Phys. Rev. B* **2003,** 68, 035416.

(24) Roke, S.; Bonn, M.; Petukhov, A. V. *Phys. Rev. B* **2004,** 70, 115106.

(25) Teich, M. C.; Saleh, B. E. A. *Fundamentals of Photonics;* Wiley: New Jersey, 2007.

(26) Boyd, R. W. *Nonlinear Optics;* Academic Press, 2003.

(27) Hache, F.; Ricard, D.; Flytzanis, C.; Kreibig, U. *Appl. Phys. A* **1988,** 47, 347-357.

(28) Ishiguro, Y.; Hayakawa, R.; Chikyow, T.; Wakayama, Y. *J. Mater.Chem. C* **2013**, 1, 3012-3016.

(29) Kumar, S.; van Herpt, J. T.; Gengler, R. Y. N.; Feringa, B. L.; Rudolf, P.; Chiechi, R. C. *J. Am. Chem. Soc.* **2016**, 138, 12519-12526.

(30) O'Brien, K.; Suchowski, H.; Rho, J.; Salandrino, A.; Kante, B.; Yin, X.; Zhang, X. *Nat. Mater.* **2015,** 14, 379-383.